An SIS-based Sideband-Separating Heterodyne Mixer Optimized for the 600 to 720 GHz Band.

F. P. Mena[(1)], J. W. Kooi[(2)], A. M. Baryshev[(1)], C. F. J. Lodewijk[(3)], R. Hesper[(2)], W. Wild[(2)], and T. M. Klapwijk[(3)].

(1) SRON Netherlands Institute for Space Research and the Kapteyn Institute of the University of Groningen, Landleven 12, 9747AD Groningen, The Netherlands.
E-mail corresponding author: f.p.mena@sron.nl

(2) California Institute of Technology, MS 320-47 Pasadena, California 91125, USA

(3) Kavli Institute of Nanoscience, Delft University of Technology, Lorentzweg 1, 2628 CJ Delft, The Netherlands.

***Abstract* - The Atacama Large Millimeter Array (ALMA) is the largest radio astronomical enterprise ever proposed. When completed, each of its 64 constituent radio-telescopes will include 10 heterodyne receivers covering the spectral windows allowed by the atmospheric transmission at ALMA's construction site, the altiplanos of the northern Chilean Andes. In contrast to the sideband-separating receivers being developed at low frequencies, double-sideband receivers are being developed for the highest two spectral windows (bands 9 and 10). Despite the well known advantages of sideband-separating mixers over their double-sideband counterparts, they have not been implemented in the highest-frequency bands, because of the very small dimensions required for some of the radio frequency components. However, advances in state-of-the-art micromachining technology now allow the structures necessary for this development to be realized. Here we report the design, modelling, realization, and characterization of a sideband-separating mixer for band 9 of ALMA (600 to 720 GHz). At the heart of the mixer, two superconductor-insulator-superconductor junctions are used as mixing elements. The constructed mixer yields excellent performance as shown by two important figures of merit: the system noise temperature and the side band ratio, both of which are within ALMA specifications at most operating frequencies.**

Manuscript received November 26, 2007; accepted January 7, 2008. Reference ST19, Category 4.
Paper submitted to Proceedings of EUCAS 2007; published in JPCS **98** (2008), paper # 012331

I. INTRODUCTION

A well known mode of detection of radio frequencies (RF) is the heterodyne principle. In its most elemental configuration, known as double-sideband (DSB) detection, the RF signal to be detected is mixed, in a non-linear device, with a signal of well-determined reference or local oscillator (LO). As a result, the RF signal is down converted to an intermediate frequency (IF) which is equal to their difference, $\omega_{IF} = |\omega_{RF} - \omega_{LO}|$. This down conversion allows further study of the signal in a more manageable frequency range (usually a few GHz). It is evident, however, that DSB mixers cannot distinguish between signals above or below the reference or local oscillator signal. Indeed, DSB mixers down convert signals above and below the LO signal (in the Upper and Lower Side Bands, or USB and LSB) to the same intermediate frequency range. It is, therefore, necessary to suppress one of the RF bands before it is fed into the mixer. This requires extra instrumentation. A well known solution is a side-band separating (2SB) mixer, which produces two IF outputs corresponding to the two RF bands (LSB and USB), without requiring additional components in front of the mixer. This solution, however, does require extra RF components in the mixer, as shown in Figure 1.

These extra components become prohibitively small at high frequencies. However, advances in micromachining technology allow them to be realized for frequencies as high as 600 GHz. Indeed, here we report the design, modelling, realization, and characterization of a 2SB mixer for frequencies from 600 to 720 GHz corresponding to band 9 of ALMA [1].

II. DESIGN AND MODELLING

A. General Concept

From a variety of possible 2SB schemes, we have selected the configuration shown in Figure 1. The RF signal to be detected is coupled to a hybrid which separates the signal into two branches of equal amplitude but with a phase separation of 90°. Each branch is coupled with the LO signal and mixed in a non-linear device. Here we use superconducting-insulator-superconducting (SIS) junctions as non-linear elements. The two resulting IF signals are coupled to a second 90° hybrid, after which two new IF signals are obtained, corresponding to the USB and LSB, respectively.

We have opted for waveguide technology for the construction of the RF components and planar stripline for the IF filtering and matching parts. Each of the RF components and the planar IF system were modeled independently using commercial microwave-analysis software (Microwave Studio*). The dimensions of each RF component were adjusted for optimal performance in the 600–720 GHz range, while the IF components are optimized for 4–8 GHz.

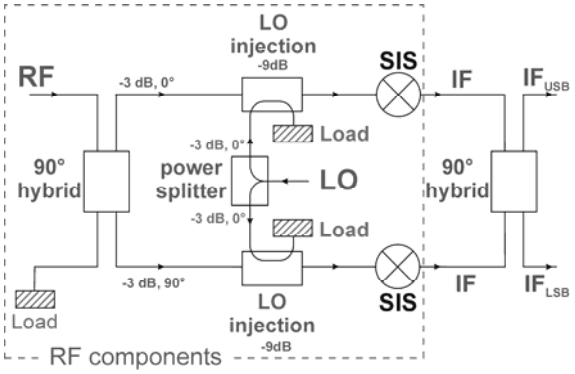

Fig. 1. Schematics of the selected 2SB configuration. The incoming RF signal is divided in a 90° hybrid. The split signals are combined with an LO signal and then mixed into two SIS junctions. The resulting down converted signals are fed into a second hybrid after which the IF signals corresponding to the lower and upper sideband are obtained in two different channels.

B. RF components

The design of the power divider, LO injectors, and 90° hybrid shown in Figure 2(a), are based on a narrow waveguide split block version developed for the ALMA project at lower frequencies [2]. Here, the waveguide widths in the hybrid and the LO injectors have been increased by 32.5% to maximize the thickness of branch lines [3]. Each of these components was simulated and optimized using commercial software. The results, summarized in Figure 3(a), show a rather flat response of the components in our frequency range.

We have selected a rather simple configuration for the terminating loads. The design consists of a cavity at the end of the waveguide partially filled with an absorbing material as shown in Figure 2(b). Since the longest dimensions of this geometry are parallel to the splitting plane of the block, this cavity and the filling material are relatively easy to machine as compared with other geometries [4]. Extensive simulations of this configuration have been

* Computation Simulation Technology, http://www.cst.com .

presented elsewhere [5]. Using Eccosorb MF112[†] as an absorbing material [5], the terminating load shows good performance, as demonstrated by the reflection coefficient presented in Figure 3(b).

We use a full-height waveguide-to-microstrip transition to couple the incoming signal to the thin-film tuning structure of the SIS junction as shown in detail in Figure 2(c). We have opted for a configuration in which the chip containing the SIS junction crosses the waveguide. To connect the DC/IF contact opposite to the radial probe we have selected a high-impedance line meandering across the waveguide [7]. In this situation, care must be taken in the way this line meanders across the waveguide as this structure is prone to generate resonances. An important modification is that we have added a capacitive step in front of the radial probe as it improves the overall performance [3]. For the RF choke we selected the popular "rectangular" structure. The calculated coupling efficiency and return loss, between the waveguide and the tip of the radial probe, are presented in Fig. 3(c).

Given the calculated S-matrices of the different RF components, we used a circuit simulator to calculate the mixer's sideband ratio (SBR), *i.e.* the ratio between the two IF output channels, of the complete RF core. The results are given in Figure 4. If a perfect IF hybrid is assumed, a SBR above 20 dB is expected across the whole band. This sets the upper limit for the performance of the present mixer.

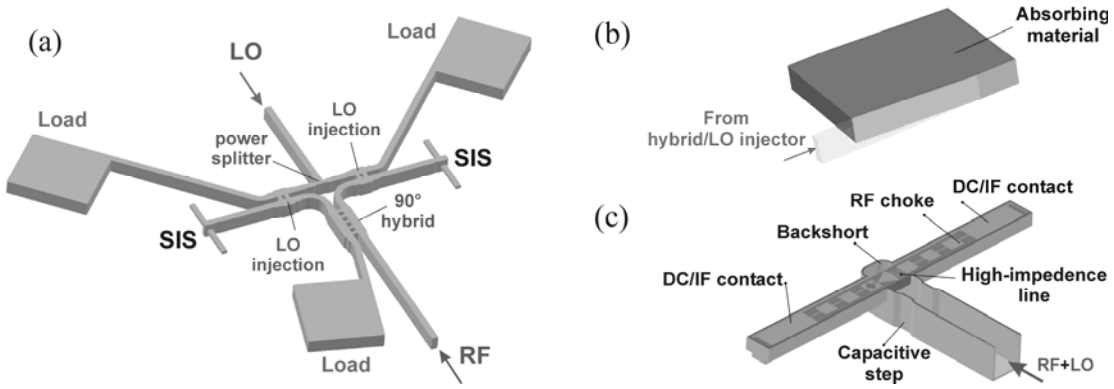

Fig. 2. Design of the RF components indicated in Figure 1: (a) The different components are designed in waveguide and, therefore, represent the channels to be machined out in the final split-block. Note that part of the split RF signal and part of the injected LO are dumped in termination loads. The transverse dimensions of the main waveguide are 145×310 μm^2. (b) Detailed view of the terminating load. (c) Detailed view of the waveguide-to-SIS transition. The function of the different components is explained in the text. All figures are drawn to scale.

C. SIS junction and tuning structure

Based on our successful experience with the development of DSB receivers for band 9 of ALMA, we have opted for single Nb/AlO_x/Nb junction devices as detector elements for our receiver. Although junctions using AlN as a barrier have intrinsically better properties [8], we have selected the former as, at the moment, its fabrication process is more reliable. The reasons for which the single junction approach is preferred are two-fold. First, it permits an easier suppression of the Josephson currents across the junction and, second, it allows less effort in finding reasonably matched mixers.

Given the resistance-area product, R_nA, of AlO_x junctions (~20 Ω.μm^2), we have selected the area of the SIS junction to be 1 μm^2 [9]. The resulting SIS impedance has to be matched

[†] Emerson & Cuming, http://www.eccosorb.com.

with the impedance at the radial probe tip which is calculated through the S-parameters given in Figure 3(c). The matching is obtained by a multisection stripline made of Nb. For a given stripline geometry, it is possible to calculate the total transmission from the radial probe tip to the SIS junction using the microscopic theory of superconductivity in the dirty limit and standard transmission line theory [5]. The geometrical parameters were tuned to get a good coverage of band 9. The result of the calculation is shown by the thick solid line in Figure 5.

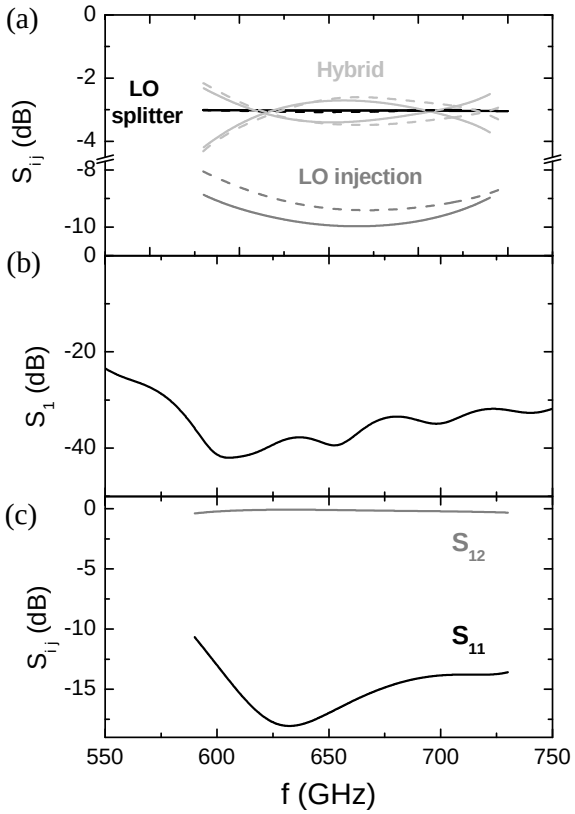

Fig. 3. Results of the electro-magnetic simulation of the different RF components: (a) S-parameters between the input and output of the 90° hybrid, LO splitter, and LO injector as designed (solid lines) and as constructed (dashed lines). (b) Reflection coefficient of the signal terminating load. (c) Coupling efficiency and return loss of the waveguide-microstrip transition.

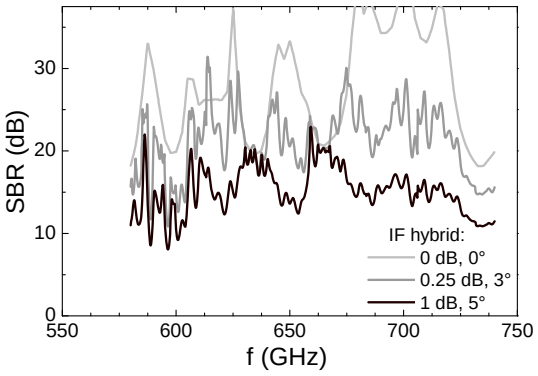

Fig. 4. Calculated SBR assuming a perfect IF hybrid (light gray) and with amplitude and phase imbalances of 0.25 dB and 3° (gray), and 1 dB and 5° (black).

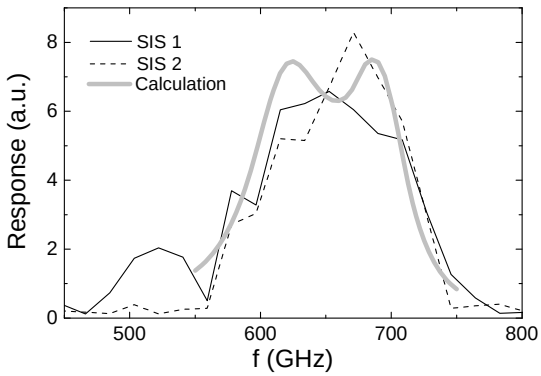

Fig. 5. Calculated and measured response of the fabricated SIS junctions. The response was measured through the RF port.

D. Planar IF filtering and matching

To facilitate reliability and modeling, we have opted for a planar IF filtering and matching design (inset of Figure 6). This is a compact unit containing the IF match, DC-break, bias tee, and EMI filter. It has to be noted that, for this filter to work, the ground plane directly underneath the filter has to be removed. The dimensions were optimized for good performance in the 4 to 8 GHz frequency range. In the main frame of Figure 6, we show the calculated performance of the IF circuit.

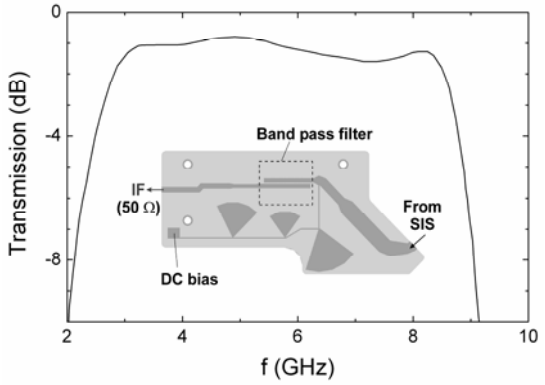

Fig. 6. Calculated transmission between the input and output ports of the IF structure presented in the inset.

III. CONSTRUCTION

A. Waveguide block

We have constructed the mixer in a split-block (Figure 7). Conventional machining was used for the large features and CNC micromachining for the small RF features [11]. Both parts of the block were made of copper which was then gold plated with a thickness of ~2 μm. The fabricated unit is rather compact (8×2×3 cm^3). It contains all the RF components, the IF filter board, the DC bias circuit, and the magnetic probes needed to suppress the Josephson currents in the SIS junctions. A closer inspection of the fabricated block shows that all the waveguides and cavities are approximately 5 μm wider than designed. The reason appears to be etching of the copper block during the gold plating process. However, the erosion is rather uniform through the entire block. We have repeated the simulation process with the measured dimensions [dashed lines in Fig. 3(a)]. It is clear that our design is pretty robust as long as the symmetry of the RF components is maintained.

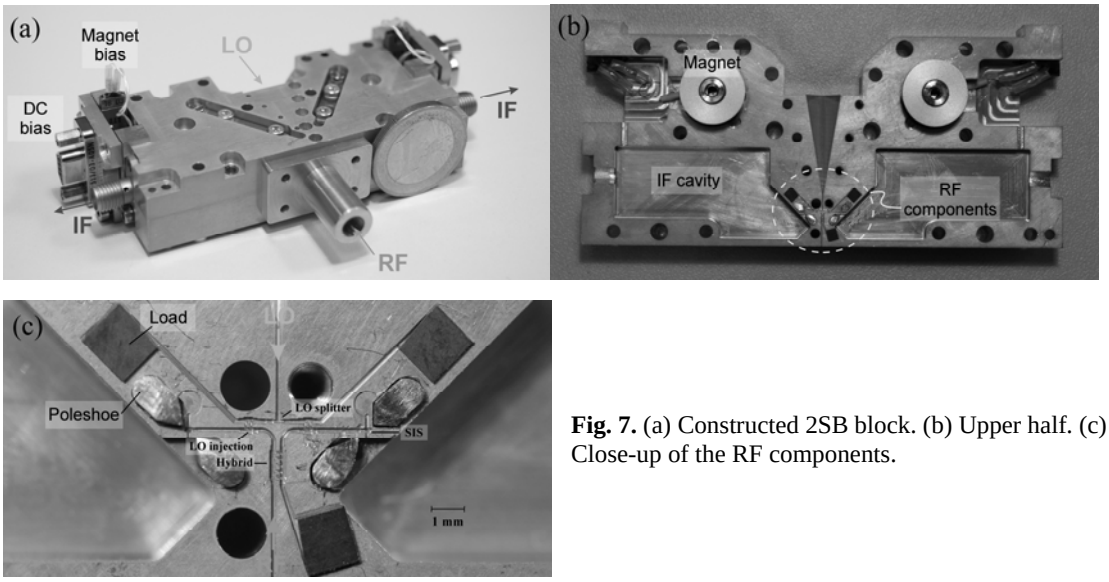

Fig. 7. (a) Constructed 2SB block. (b) Upper half. (c) Close-up of the RF components.

B. SIS junctions

The SIS devices were fabricated on a quartz substrate. First, a Nb monitor layer was deposited, after which an optically defined ground plane pattern of Nb/Al/AlO_x/Nb was lifted off. Junctions were defined by e-beam lithography in a negative e-beam resist layer and etched out with a SF_6/O_2 reactive ion etch (RIE) using AlO_x as an etch stop. The junction resist pattern was subsequently used as a lift-off mask for a dielectric layer of SiO_2. A Nb/Au top layer was deposited and Au was etched with a wet etch in a KI/I2 solution using an optically defined mask. Finally, using an e-beam defined top wire mask pattern, the layer of Nb was etched with a SF_6/O_2 RIE, finishing the fabrication process. This process renders a high yield and good reproducibility as demonstrated by the I-V plots of 8 junctions (out of a sector containing 20 junctions) shown in Figure 8.

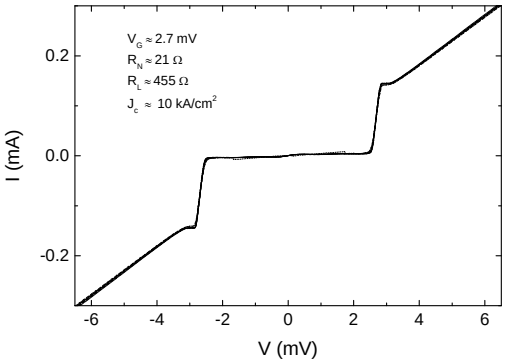

Fig. 8. I-V curves of 8 different junctions. The average values of gap voltage (V_G), normal resistance (R_N), leakage resistance (R_L), and critical current density (J_C) are shown.

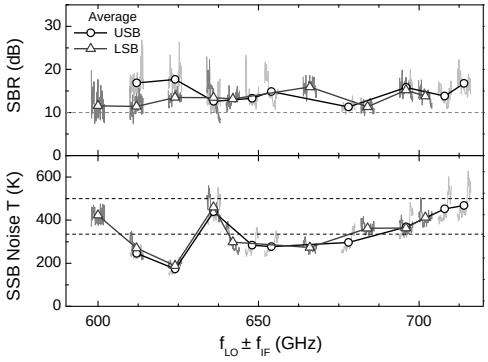

Fig. 9. Single sideband noise temperatures (bottom panel) and image rejection ratios (upper panel) at different LO frequencies. Both parameters are close to ALMA specifications (horizontal dashed lines), as described in the text.

IV. CHARACTERIZATION

A. Band coverage

The direct response, as function of frequency, of both SIS junctions contained in our mixer has been measured using a home-made Fourier transform spectrometer. The results are presented in Figure 5. Both junctions present good band coverage and are in good agreement with the predicted response.

B. Noise temperature and sideband ratio

Noise temperatures (T_{RX}) were measured using the conventional Y-factor method. As described in [12], the same setup was slightly modified to determine the sideband ratios. The T_{RX} and SBR for both output ports were determined at several LO pumping frequencies and recorded as a function of IF frequency. The results are summarized in Figure 9. Both quantities are rather close to the ALMA specifications, as indicated by the horizontal dashed lines. For T_{RX}, 80% of the band should not exceed 335 K while all points should be below 500 K [1]. The image rejection ratio, on the other hand, should always be above 10 dB. Although the noise temperature complies with ALMA specifications, it is obvious from Figure 9 that the IF response presents a rather steep increase at high IF frequencies. The most probable reason is a mismatch between the SIS impedance and the IF system. Further work has to be done to reduce the mismatch and improve the noise temperatures and sideband ratio.

The obtained image rejection ratios are in close agreement with the modeling prediction given in Figure 4 if amplitude and phase mismatches of 1 dB and 5° in the IF hybrid are

considered. These, indeed, are the experimental values obtained at 77 K [13]. It has to be noted that the hybrid used is a commercial one[‡] that has been optimized for operation at ambient temperature. It is reasonable to argue that mismatches of 0.25dB and 3° can be obtained by optimizing the design for low temperatures. In that case, an improvement of ~7 dB is expected (see Figure 4).

V. CONCLUSIONS

In this article we have presented the design, modeling, and realization of a side-band-separating mixer that covers the frequency range of ALMA band 9. A full test of the mixer was also presented. It was found that less than 10% of the points are below the required sideband ratio (10 dB) and above the specified noise temperature (500 K). However, further improvement can be achieved if the IF system is optimized and AlN-barrier SIS junctions are used. With these, full compliance with the ALMA specifications is expected.

REFERENCES

[1] ALMA web site, http://www.alma.nrao.edu.

[2] S.M.X Claude *et al*., Alma Memo 316 (2000). Available online at: http://www.alma.nrao.edu/memos/html-memos/abstracts/abs316.html.

[3] J. Kooi et al., *SPIE Proceedings*, Millimiter and submillimiter detectors for Astronomy II, **332**, 5498 (2004).

[4] A. Kerr et al., Alma Memo 494 (2004). Available online at: http://www.alma.nrao.edu/memos/html-memos/abstracts/abs494.html

[5] F. P. Mena and A. Baryshev, Alma Memo 513 (2005). Available online at: http://www.alma.nrao.edu/memos/html-memos/abstracts/abs513.html..

[6] G. A. Ediss et al., Alma Memo 273 (1999). Available online at: http://www.alma.nrao.edu/memos/html-memos/abstracts/abs273.html.

[7] C. Risacher *et al., IEEE Micro. and Wire. Comp. Lett.*, **13**, 262 (2003).

[8] J. Kawamura *et al*., *Appl. J. Phys*. **76**, 2119 (1996).

[9] A. R. Kerr and S.-K. Pan, Int. J. *Ir. & Mm. Waves*, **11**, 1169 (1990).

[10] C. F. J. Lodewijk et al., Conf. Proc. 16th ISSTT, p. 42 (2005). Available online at: http://www.mc2.chalmers.se/mc2/conferences/ISSTT/ISSTT2005-proceedings.pdf.

[11] Radiometer Physics GmbH, http://www.radiometer-physics.de/.

[12] A. R. Kerr, S.-K. Pan, and J. E. Effland , ALMA Memo 357 (2001). Available online at: http://www.alma.nrao.edu/memos/html-memos/abstracts/abs273.html.

[13] S. Mahieu, Institut de RadioAstronomie Millimétrique, France, priv. comm., Jan. 2006.

[‡] Advanced Technical Materials Inc., http://www.atmmicrowave.com/.